Robust Quantum Memory in a Trapped-Ion Quantum Network Node

P. Drmota, D. Main, D. P. Nadlinger, B. C. Nichol, M. A. Weber, E. M. Ainley, A. Agrawal, R. Srinivas, G. Araneda, C. J. Ballance, and D. M. Lucas

Robust Quantum Memory in a Trapped-Ion Quantum Network Node

P. Drmota,* D. Main, D. P. Nadlinger, B. C. Nichol, M. A. Weber, E. M. Ainley,
A. Agrawal, R. Srinivas, G. Araneda, C. J. Ballance, and D. M. Lucas

Department of Physics, University of Oxford, Clarendon Laboratory,
Parks Road, Oxford OX1 3PU, United Kingdom

We integrate a long-lived memory qubit into a mixed-species trapped-ion quantum network node. Ion-photon entanglement first generated with a network qubit in $^{88}\text{Sr}^+$ is transferred to $^{43}\text{Ca}^+$ with 0.977(7) fidelity, and mapped to a robust memory qubit. We then entangle the network qubit with another photon, which does not affect the memory qubit. We perform quantum state tomography to show that the fidelity of ion-photon entanglement decays ~ 70 times slower on the memory qubit. Dynamical decoupling further extends the storage time; we measure an ion-photon entanglement fidelity of 0.81(4) after 10 s.

Quantum networks have the potential to revolutionize the way we distribute and process information [1]. They have applications in cryptography [2, 3], quantum computing [4, 5], metrology [6], and can provide insights into the nature of entanglement [7, 8]. Photonic interfaces are essential for such networks, enabling two remote stationary qubits to exchange quantum information using entanglement swapping [9]. Elementary quantum networks have been realized with diamond nitrogen-vacancy centers [8, 10], photonics [11, 12], neutral atoms [13, 14], in solid state systems [15], and trapped ions [7, 16–24].

Trapped ions provide qubits with exceptionally long coherence times, which can be initialized, manipulated, entangled and read out with high fidelity [25–30]. Moreover, trapped ions readily interact with optical fields, providing a natural interface between their electronic state – the stationary quantum memory – and photons – the "flying" quantum information carrier [31]. Pairs of trapped-ion network nodes comprising one qubit of a single species have been connected by a photonic link and used to perform Bell tests [7], state teleportation [18], random number generation [19], quantum key distribution [21], and frequency comparisons [22]. Trapped ion systems have also demonstrated state-of-the-art single- and two-qubit gate fidelities, but integrating these within a quantum network node remains a challenge since an ion species suitable for quantum communication does not necessarily also provide a good memory qubit with sufficient isolation from network activity. Atomic species such as $^{133}\text{Ba}^+$ or $^{171}\text{Yb}^+$ have been proposed to circumvent this issue [26, 32], however, the development of the required experimental techniques is still ongoing. Nevertheless, it is possible for each role to be fulfilled by a different species [33]. In addition, using multiple atomic species has advantages for minimizing crosstalk during mid-circuit measurements and cooling [34].

In this Letter, we demonstrate a trapped-ion quantum network node in which entanglement between a network qubit and a photon is created and coherently transferred onto a memory qubit for storage, while the network qubit is entangled with a second photon. Due to its simple level structure, $^{88}\text{Sr}^+$ is ideally suited for our ion-photon entanglement (IPE) scheme [20], whereas the hyperfine structure of $^{43}\text{Ca}^+$ provides a long-lived memory qubit [35]. While both IPE and local mixed-species entangling gates have been demonstrated independently [33], this is the first experiment in which these capabilities are combined. Furthermore, we show that the memory qubit in $^{43}\text{Ca}^+$ is robust to environmental noise as well as concurrent addressing of $^{88}\text{Sr}^+$ for the generation of IPE. Finally, sympathetic cooling of the ion chain using $^{88}\text{Sr}^+$ between rounds of entanglement generation enables continued operation even in the presence of heating.

For this experiment, we load a $^{88}\text{Sr}^+$-$^{43}\text{Ca}^+$ crystal with controlled order into a surface-electrode Paul trap at room temperature [36]. Each experimental sequence begins with cooling [37], reducing the temperature of the axial out-of-phase (OOP) and in-phase (IP) motion to $\bar{n}_\text{oop} \simeq 0.3$ and $\bar{n}_\text{ip} \simeq 3$, respectively. The cooling sequence was empirically optimized for the high heating rates observed, namely $\dot{\bar{n}}_\text{oop} \simeq 360\,\text{s}^{-1}$ at $\omega_\text{oop}/(2\pi) = 3.354\,\text{MHz}$ and $\dot{\bar{n}}_\text{ip} \simeq 2700\,\text{s}^{-1}$ at $\omega_\text{ip}/(2\pi) = 1.705\,\text{MHz}$. To produce single photons, $^{88}\text{Sr}^+$ is excited to the $\left|P_{1/2},\, m_J = +1/2\right\rangle$ state by a $\sim 10\,\text{ps}$ laser pulse. This short-lived excited state decays with probability 0.95 into the $S_{1/2}$ manifold via emission of a photon at 422 nm whose polarization is entangled with the spin state of the ion. The photon emission is imaged by an NA = 0.6 objective onto a single-mode optical fiber [Fig. 1(a)], which acts as a spatial mode filter, maximizing the entangled fraction by suppressing polarization mixing. The ion-photon state can then be described by the maximally-entangled Bell state

$$|\psi\rangle = \tfrac{1}{\sqrt{2}} \left(|{\downarrow}_\text{N}\rangle \otimes |H\rangle + |{\uparrow}_\text{N}\rangle \otimes |V\rangle \right) ,$$

where $|H\rangle$ and $|V\rangle$ are orthogonal linear polarization states of the photon, and $|{\downarrow}_\text{N}\rangle$ and $|{\uparrow}_\text{N}\rangle$ denote the network qubit states in the Zeeman ground state manifold of $^{88}\text{Sr}^+$ [Fig. 1(b)]. To analyze the polarization state of the photon, we employ polarizing beamsplitters and avalanche photodiodes, which are part of the same pho-

tonic Bell state analyzer used to herald remote entanglement between two network nodes [20]. The pulsed excitation sequence is repeated in a loop at an attempt rate of 1 MHz until a photon is detected. The polarization measurement basis is set at the beginning of a sequence using motorized waveplates. Qubit manipulation of ^{88}Sr$^+$ is performed on the 674 nm quadrupole transition, which
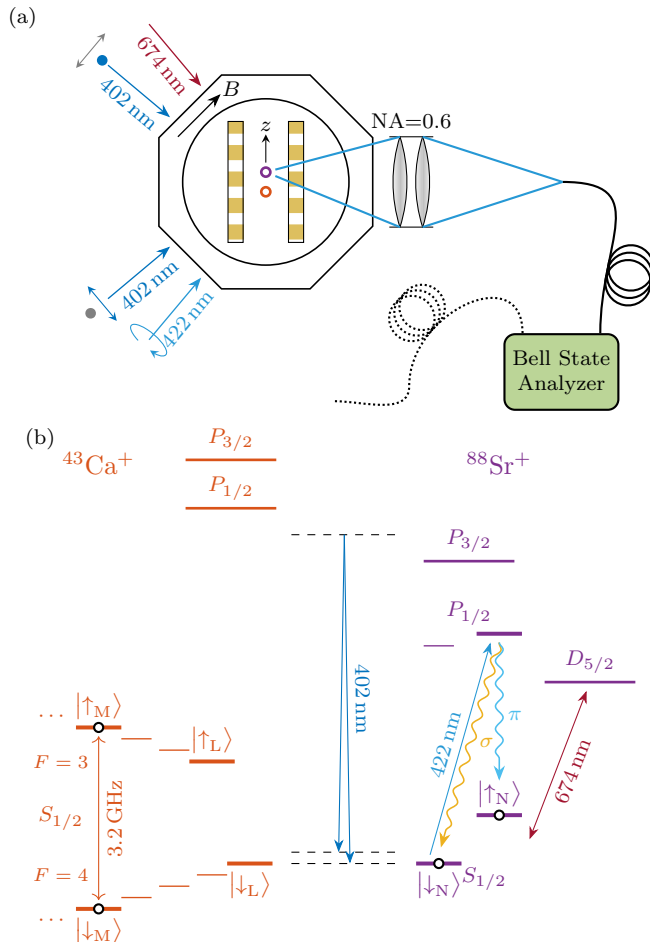

FIG. 1. (a) Overview of the apparatus. We show the laser beam geometry; within the plane of the trap surface, the magnetic field B is oriented 45 deg to the trap axis z. Perpendicular to this plane, the NA = 0.6 lens collects single photons from a ^{88}Sr$^+$ ion (violet circle). Single photons are coupled into a single-mode fiber that is connected to a Bell state analyzer. Here, only one network node is connected; the same device can herald remote entanglement with a second, identical node [20]. The state of ^{88}Sr$^+$ can be mapped onto a co-trapped ^{43}Ca$^+$ ion (orange circle). (b) Level structure of ^{88}Sr$^+$ (violet) and ^{43}Ca$^+$ (orange), not to scale. The memory qubit comprises the $m_F = 0$ states in the ^{43}Ca$^+$ $S_{1/2}$ manifold. Raman lasers (blue arrows) are used to drive mixed-species entangling gates and transitions between ^{43}Ca$^+$ hyperfine ground states. A σ^+-polarized laser pulse excites the $S_{1/2} \leftrightarrow P_{1/2}$ transition in ^{88}Sr$^+$ to generate a single photon whose polarization (see σ and π decay channels) is entangled with the state of the ion. A narrow-linewidth quadrupole laser (red arrow) is used to manipulate the ^{88}Sr$^+$ qubit.

is also used for electron shelving readout.

The second ion species, ^{43}Ca$^+$, is chosen for its excellent coherence properties and the high level of control achieved in previous experiments [27, 38–40]. Furthermore, the mass ratio between ^{43}Ca$^+$ and ^{88}Sr$^+$ is reasonably favorable for sympathetic cooling [41] and the electronic level structure facilitates mixed-species gates [42]. For state preparation, polarized 397 nm light optically pumps population into $|\downarrow_L\rangle$. A pair of co-propagating Raman laser beams at $\lambda_R = 402$ nm is used to manipulate states within the ground state manifold. For readout, population is shelved using a pulse sequence of 393 nm and 850 nm light [43]. At a magnetic field of 0.5 mT, the frequency of the memory qubit transition depends weakly on the magnetic field magnitude, with a sensitivity of 122 kHz mT^{-1}. Compared to the sensitivity of the ^{88}Sr$^+$ Zeeman qubit of 28 MHz mT^{-1}, the memory qubit is significantly more resilient to magnetic field noise. In addition, the magnetic field at the position of the ions is actively stabilized using feedback and feedforward currents to the 10 nT level, calibrated over the 50 Hz line cycle using ^{88}Sr$^+$ as a magnetic field probe [44].

To swap information from ^{88}Sr$^+$ to ^{43}Ca$^+$, we perform mixed-species $\hat{\sigma}_z \otimes \hat{\sigma}_z$ geometric phase gates using the state-dependent light shift force generated by a single pair of ~ 20 mW Raman laser beams at 402 nm. Only one pair is required to drive both species thanks to their compatible electronic level structure [42] [Fig. 1(b)]. The main advantage of this scheme over Cirac-Zoller and Mølmer-Sørensen gates, which have previously been explored in this context [33, 45], is its robustness to qubit frequency shifts. The Raman beams are aligned to address the OOP axial motion of the two-ion crystal [42]. For maximum gate efficiency on this mode, the ion spacing is set to a half-integer multiple of the effective wavelength $\lambda_R/\sqrt{2}$. As the memory qubit in ^{43}Ca$^+$ does not experience a light shift, this interaction is performed on the logic qubit instead. First-order Walsh modulation compensates for the light shift imbalance between the two species. With the available laser power, a detuning of $\delta/(2\pi) = 34$ kHz from the OOP mode achieves a gate duration of ≈ 60 μs while minimizing off-resonant excitation of the IP mode [37]. Charging of the trap due to the Raman laser beams is automatically compensated every ~ 5 min using the method described in Ref. [46].

The state of the network qubit in ^{88}Sr$^+$ is coherently swapped onto the logic qubit using an iSWAP gate, which is implemented by two $\hat{\sigma}_z \otimes \hat{\sigma}_z$ interactions and single-qubit rotations [circuit shown in Fig. 2(a)]. We use the iSWAP, as opposed to a full SWAP, since the initial state of ^{43}Ca$^+$ is known to be prepared in $|\downarrow_L\rangle$. The ideal iSWAP performs the mapping $|\phi_N\rangle \otimes |\downarrow_L\rangle \mapsto |\downarrow_N\rangle \otimes |\phi_L\rangle$, where $|\phi\rangle$ is the arbitrary state to be swapped to the logic qubit, leaving the network qubit in the $|\downarrow_N\rangle$ state. Experimental imperfections leading to deviations from
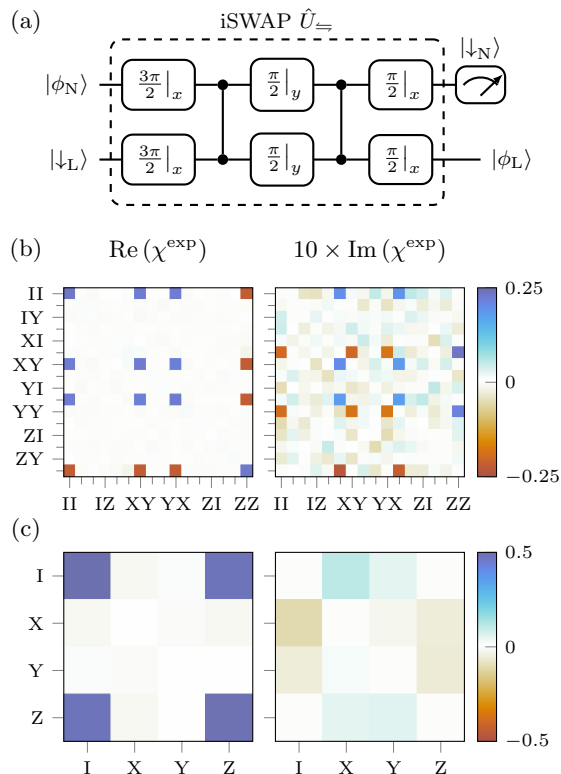
FIG. 2. (a) The iSWAP circuit used to map the network qubit state from ^{88}Sr$^+$ to the logic qubit in ^{43}Ca$^+$. (b) The Choi matrix reconstructed from process tomography of the iSWAP gate before error detection indicates a process fidelity of 0.913(3). (c) Initializing the logic qubit in $|{\downarrow_L}\rangle$ and rejecting errors flagged by the measurement on the network qubit, the fidelity of this conditional process is 0.977(7).

the target subspace $|{\downarrow_N}\rangle\langle{\downarrow_N}| \otimes \hat{1}_L$ are detected via a mid-circuit measurement on the network qubit [47]. We characterize the iSWAP operation independently using process tomography [48, 49] to reconstruct the Choi process matrix χ^{exp} and calculate the process fidelity $\mathcal{F}_p = \mathrm{Tr}(\chi^{\mathrm{id}}\chi^{\mathrm{exp}})$ with respect to the ideal process χ^{id}, yielding 0.913(3) [Fig. 2(b)]. Considering only the mapping from the subspace $\hat{1}_N \otimes |{\downarrow_L}\rangle\langle{\downarrow_L}|$ where the logic qubit is prepared in $|{\downarrow_L}\rangle$ to the subspace $|{\downarrow_N}\rangle\langle{\downarrow_N}| \otimes \hat{1}_L$ where the network qubit is measured in $|{\downarrow_N}\rangle$, the process fidelity is 0.977(7) with respect to the ideal process $|\phi_N\rangle \otimes |{\downarrow_L}\rangle \mapsto |{\downarrow_N}\rangle \otimes |\phi_L\rangle$ [Fig. 2(c)].

The iSWAP operation enables the transfer of IPE from the network qubit in ^{88}Sr$^+$ to the memory qubit in ^{43}Ca$^+$, so that IPE can be created a second time using ^{88}Sr$^+$. To probe the memory properties of the integrated system of entangled photons and ions, we perform tomography on both ion-photon states in parallel after a variable storage duration. For this, we initialize $|{\downarrow_L}\rangle \otimes |{\downarrow_N}\rangle$ and execute the attempt loop until a single photon is detected [point I in Fig. 3(a)]. Subsequently, we swap the network qubit state to the logic qubit, and further to the

memory qubit for storage [37]. If the 130 μs mid-circuit measurement on the network qubit indicates a success [point II in Fig. 3(a)], the attempt loop is executed until a second photon is detected [point III in Fig. 3(a)]. After a variable delay Δt, both the memory and the network qubit are measured. Note that no dynamical decoupling is used throughout this sequence. Figure 3(c) shows the fidelity of ion-photon states to the closest maximally entangled state [50] for different storage times. The raw ^{88}Sr$^+$-photon fidelity is 0.97(2), but dephasing of the network qubit limits the coherence time of this state to 2 ms. Swapping the ion state into the memory qubit extends the coherence time by a factor ~ 70 with an initial fidelity of 0.93(2). The additional infidelity is due to the high heating rates limiting the iSWAP operation [37], and imperfections in the L → M transfer pulse sequence [37]. The fidelity shown in Fig. 3(c) decays due to magnetic field noise and laser leakage; heating during the storage duration causes single-qubit rotation errors in ^{88}Sr$^+$, whereas the Raman beam geometry eliminates this effect in ^{43}Ca$^+$.

In a second experiment, we demonstrate that these limitations can be overcome. We employ Knill dynamical decoupling [25, 51] with 40 spin flips to suppress the effect of magnetic field noise [Fig. 3(b)]. To minimize the effect of laser leakage, we transport the ions 100 μm away from the laser interaction zone. Furthermore, sympathetic Doppler cooling on ^{88}Sr$^+$ avoids ion loss due to heating. We achieve an IPE fidelity of 0.81(4) after 10 s [squares and inset in Fig. 3(c)]. The ratio of decoherence rate to the node-to-node entanglement rate in a quantum network impacts the resource scaling for fault-tolerant error correction [52]. Here, this ratio is estimated to be 0.0006 and 0.08 with and without dynamical decoupling, respectively, assuming the entanglement rate of 182 s^{-1} previously observed in our setup [20].

Crucially, there is negligible error associated with generating a second ion-photon pair, as the lasers used during the attempt loop are far off-resonant ($> $ THz) from transitions in ^{43}Ca$^+$. To demonstrate this, we perform Ramsey experiments on the memory qubit while the loop is ongoing in the background for up to 10^5 excitation attempts [Fig. 4(a) and Fig. 4(b)], enough to herald > 1500 entangled ion-photon states. The light shift per excitation attempt is 8.8(6) μrad, and can easily be corrected in real-time by adjusting the phase reference. From the same data, we do not observe any statistically significant reduction in contrast [Fig. 4(b)]. A secondary consequence of the loop is excess heating due to photon recoil. We measure excess heating of $9.3(9) \times 10^{-4}$ phonons per attempt [Fig. 4(c)], which is insignificant in the context of this experiment [Fig. 4(d)].

In summary, we have demonstrated the coherent transfer of IPE from a network qubit in ^{88}Sr$^+$ to a memory qubit in ^{43}Ca$^+$ within a quantum network node. We note that the measurements reveal the presence of entangle-

(a)

Photon

$^{88}\text{Sr}^+$ N

$^{43}\text{Ca}^+$ { L, M

$\hat{U}_{\rightleftharpoons}$

Δt

Δt

(b)

$^{88}\text{Sr}^+$ N

$^{43}\text{Ca}^+$ M

Cooling

$\left(\text{DD} - \frac{3\pi}{2} - \text{DD} - \frac{\pi}{2} \right)^4$

$-\frac{\tau}{2}- \boxed{\pi|_{\frac{2\pi}{3}}} -\tau- \boxed{\pi|_{\frac{\pi}{2}}} -\tau- \boxed{\pi|_{\pi}} -\tau- \boxed{\pi|_{\frac{\pi}{2}}} -\tau- \boxed{\pi|_{\frac{2\pi}{3}}} -\frac{\tau}{2}-$

(c)

$^{43}\text{Ca}^+$ Memory   (+dyn. decoupl.)

$^{88}\text{Sr}^+$ Network

Ion-photon entanglement fidelity
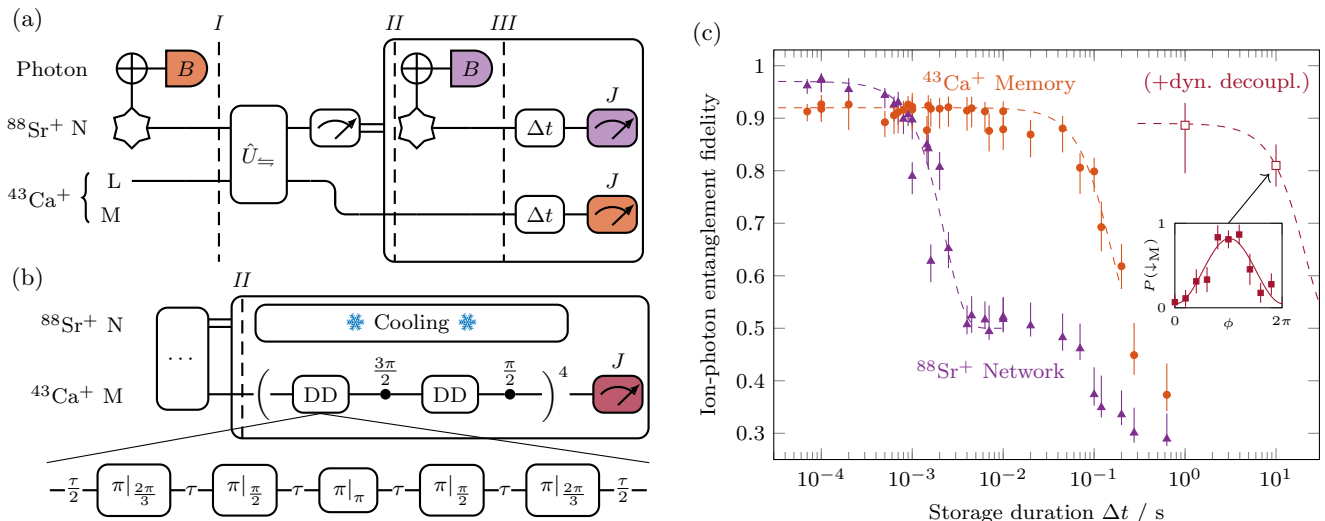
Storage duration Δt / s

$P(\downarrow_M)$

FIG. 3. (a-b) Experimental sequences to probe the memory properties of the network node. Delayed measurements from a complete set of bases $B \otimes J$ are used to tomographically reconstruct the density matrices of the ion-photon states. If the mid-circuit measurement detects errors in the iSWAP gate, the sequence is immediately restarted. (a) A second photon is generated after transferring the state entangled with the first photon to the memory qubit. (b) After transferring IPE from the network qubit to the memory qubit, $^{88}\text{Sr}^+$ is used to sympathetically cool $^{43}\text{Ca}^+$. Dynamical decoupling and ion transport are used to extend the memory coherence time during the storage period. (c) The fidelities of the ion-photon states with respect to the closest maximally entangled state [37] are calculated from the density matrix obtained from maximum likelihood estimation [37] and averaged over all four photon detectors. Error bars span the 95% confidence interval obtained from nonparametric bootstrapping [37]. Dashed curves show Gaussian decay models to guide the eye. Square marks indicate the fidelity with dynamical decoupling, ion transport, and sympathetic cooling using $^{88}\text{Sr}^+$ during the storage time. At $10\,\text{s}$, only the populations and the parity (see inset for the signal correlated with one photon detector with varying memory qubit rotation angle ϕ) were measured to infer the fidelity.

ment even though the photon was destroyed before the transfer took place [53]. We extend the storage duration of this entanglement by ~ 2 orders of magnitude, while ensuring that subsequent IPE can be performed without crosstalk affecting the memory qubit. Using dynamical decoupling, we achieve a storage duration exceeding $10\,\text{s}$. Extending the storage duration beyond the time taken to generate IPE is essential for applications that require multiple communication photons. We have shown that we can generate further IPE on the network qubit while maintaining coherence on a memory qubit $3.3\,\mu\text{m}$ away – this enables applications such as entanglement distillation [54–56] and blind quantum computing [57]. Mixed-species transfer in a network node also enables applications that require remote entanglement of long-lived memories, including quantum networks of atomic clocks [6, 22]. For long-distance networks, communication latencies due to time-of-flight and classical signaling would limit the rate at which nodes with a single network qubit can generate entanglement. However, if the state of this network qubit is stored in an available memory qubit immediately after emission of the photon, entanglement attempts could be made without dead-time in between [24]. A constant attempt rate could be reached independent of distance, limited only by the local swapping procedure. In that scheme, the memory

qubits would be stored until the corresponding herald signals arrive to indicate which had been entangled successfully. In our system, link losses, rather than memory coherence, would set the limit on the maximum possible node separation. To increase the photon collection efficiency, cavities can be used [23, 58]. To reduce the fiber losses, quantum frequency conversion to infrared wavelengths has been proven feasible [59–61]. Combined with these improvements, our system integrating a high-fidelity photonic interface with mixed-species quantum logic, a robust memory and ion transport capabilities, paves the way for more powerful trapped-ion quantum networks.
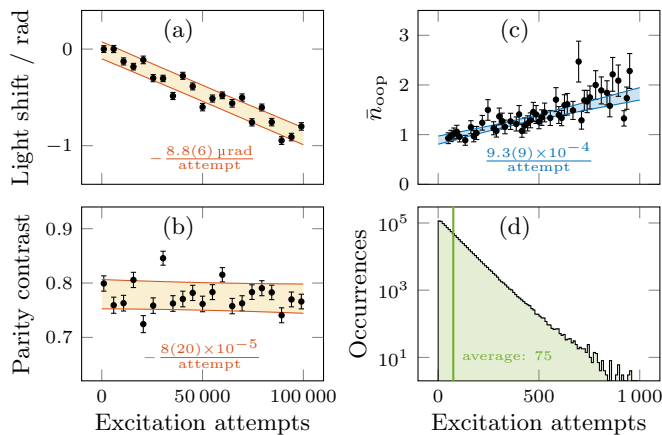
FIG. 4. The effect of excitation attempts on (a) the phase and (b) coherence of the memory qubit, and (c) the temperature of the OOP mode, is probed by executing the attempt loop for a variable fraction of a fixed total duration. Each attempt takes 1 μs. The sensitivity to attempts, extracted from linear least-squares fits, is shown alongside the data. Error intervals span one standard deviation. (a-b) Ramsey experiments with 100 ms total duration. Filled single-prediction bands guide the eye to (a) phase and (b) contrast of the parity signal. (c) Sideband-ratio thermometry with 1 ms total duration. The 95 % confidence band is shown in blue. (d) Histogram of excitation attempts until detection of a photon, indicating a success probability of 0.013.

0340).

* peter.drmota@physics.ox.ac.uk

[1] H. J. Kimble, The quantum internet, Nature **453**, 1023 (2008).

[2] C. H. Bennett and G. Brassard, Quantum cryptography: public key distribution and coin tossing, Theor. Comput. Sci. **560**, 7 (1984).

[3] A. K. Ekert, Quantum cryptography based on bell's theorem, Phys. Rev. Lett. **67**, 661 (1991).

[4] C. H. Bennett, G. Brassard, C. Crépeau, R. Jozsa, A. Peres, and W. K. Wootters, Teleporting an unknown quantum state via dual classical and einstein-podolsky-rosen channels, Phys. Rev. Lett. **70**, 1895 (1993).

[5] D. Hucul, I. V. Inlek, G. Vittorini, C. Crocker, S. Debnath, S. M. Clark, and C. Monroe, Modular entanglement of atomic qubits using photons and phonons, Nat. Phys. **11**, 37 (2015).

[6] P. Kómár, E. M. Kessler, M. Bishof, L. Jiang, A. S. Sørensen, J. Ye, and M. D. Lukin, A quantum network of clocks, Nat. Phys. **10**, 582 (2014).

[7] D. N. Matsukevich, P. Maunz, D. L. Moehring, S. Olmschenk, and C. Monroe, Bell inequality violation with two remote atomic qubits, Phys. Rev. Lett. **100**, 150404 (2008).

[8] B. Hensen, H. Bernien, A. E. Dréau, A. Reiserer, N. Kalb, M. S. Blok, J. Ruitenberg, R. F. L. Vermeulen, R. N. Schouten, C. Abellán, W. Amaya, V. Pruneri, M. W. Mitchell, M. Markham, D. J. Twitchen, D. Elkouss, S. Wehner, T. H. Taminiau, and R. Hanson, Loophole-free Bell inequality violation using electron spins separated by 1.3 kilometres, Nature **526**, 682 (2015).

[9] T. E. Northup and R. Blatt, Quantum information transfer using photons, Nat. Photon. **8**, 356 (2014).

[10] S. L. N. Hermans, M. Pompili, H. K. C. Beukers, S. Baier, J. Borregaard, and R. Hanson, Qubit teleportation between non-neighbouring nodes in a quantum network, Nature **605**, 663 (2022).

[11] T. Jennewein, C. Simon, G. Weihs, H. Weinfurter, and A. Zeilinger, Quantum cryptography with entangled photons, Phys. Rev. Lett. **84**, 4729 (2000).

[12] J. Yin, J.-G. Ren, H. Lu, Y. Cao, H.-L. Yong, Y.-P. Wu, C. Liu, S.-K. Liao, F. Zhou, Y. Jiang, X.-D. Cai, P. Xu, G.-S. Pan, J.-J. Jia, Y.-M. Huang, H. Yin, J.-Y. Wang, Y.-A. Chen, C.-Z. Peng, and J.-W. Pan, Quantum teleportation and entanglement distribution over 100-kilometre free-space channels, Nature **488**, 185 (2012).

[13] C. Nölleke, A. Neuzner, A. Reiserer, C. Hahn, G. Rempe, and S. Ritter, Efficient teleportation between remote single-atom quantum memories, Phys. Rev. Lett. **110**, 140403 (2013).

[14] W. Zhang, T. van Leent, K. Redeker, R. Garthoff, R. Schwonnek, F. Fertig, S. Eppelt, W. Rosenfeld, V. Scarani, C. C.-W. Lim, and H. Weinfurter, A device-independent quantum key distribution system for distant users, Nature **607**, 687 (2022).

[15] P. Magnard, S. Storz, P. Kurpiers, J. Schär, F. Marxer, J. Lütolf, T. Walter, J.-C. Besse, M. Gabureac, K. Reuer, A. Akin, B. Royer, A. Blais, and A. Wallraff, Microwave quantum link between superconducting circuits housed in spatially separated cryogenic systems, Phys. Rev. Lett. **125**, 260502 (2020).

[16] D. N. Matsukevich, T. Chanelière, S. D. Jenkins, S.-Y. Lan, T. A. B. Kennedy, and A. Kuzmich, Entanglement of remote atomic qubits, Phys. Rev. Lett. **96**, 030405 (2006).

[17] D. L. Moehring, P. Maunz, S. Olmschenk, K. C. Younge, D. N. Matsukevich, L.-M. Duan, and C. Monroe, Entanglement of single-atom quantum bits at a distance, Nature **449**, 68 (2007).

[18] S. Olmschenk, D. N. Matsukevich, P. Maunz, D. Hayes, L.-M. Duan, and C. Monroe, Quantum teleportation between distant matter qubits, Science **323**, 486 (2009).

[19] S. Pironio, A. Acín, S. Massar, A. B. de la Giroday, D. N. Matsukevich, P. Maunz, S. Olmschenk, D. Hayes, L. Luo, T. A. Manning, and C. Monroe, Random numbers certified by Bell's theorem, Nature **464**, 1021 (2010).

[20] L. J. Stephenson, D. P. Nadlinger, B. C. Nichol, S. An, P. Drmota, T. G. Ballance, K. Thirumalai, J. F. Goodwin, D. M. Lucas, and C. J. Ballance, High-rate, high-fidelity entanglement of qubits across an elementary quantum network, Phys. Rev. Lett. **124**, 110501 (2020).

[21] D. P. Nadlinger, P. Drmota, B. C. Nichol, G. Araneda, D. Main, R. Srinivas, D. M. Lucas, C. J. Ballance, K. Ivanov, E. Y.-Z. Tan, P. Sekatski, R. L. Urbanke, R. Renner, N. Sangouard, and J.-D. Bancal, Experimental quantum key distribution certified by Bell's theorem, Nature **607**, 682 (2022).

[22] B. C. Nichol, R. Srinivas, D. P. Nadlinger, P. Drmota, D. Main, G. Araneda, C. J. Ballance, and D. M. Lucas, An elementary quantum network of entangled optical atomic clocks, Nature **609**, 689 (2022).

[23] V. Krutyanskiy, M. Galli, V. Krcmarsky, S. Baier, D. A. Fioretto, Y. Pu, A. Mazloom, P. Sekatski, M. Canteri, M. Teller, J. Schupp, J. Bate, M. Meraner, N. Sangouard, B. P. Lanyon, and T. E. Northup, Entanglement of trapped-ion qubits separated by 230 meters (2022), arXiv:2208.14907.

[24] V. Krutyanskiy, M. Canteri, M. Meraner, J. Bate, V. Krcmarsky, J. Schupp, N. Sangouard, and B. P. Lanyon, A telecom-wavelength quantum repeater node based on a trapped-ion processor (2022), arXiv:2210.05418.

[25] P. Wang, C.-Y. Luan, M. Qiao, M. Um, J. Zhang, Y. Wang, X. Yuan, M. Gu, J. Zhang, and K. Kim, Single ion qubit with estimated coherence time exceeding one hour, Nat. Commun. **12**, 233 (2021).

[26] J. E. Christensen, D. Hucul, W. C. Campbell, and E. R. Hudson, High-fidelity manipulation of a qubit enabled by a manufactured nucleus, npj Quantum Inf. **6**, 35 (2020).

[27] T. P. Harty, D. T. C. Allcock, C. J. Ballance, L. Guidoni, H. A. Janacek, N. M. Linke, D. N. Stacey, and D. M. Lucas, High-fidelity preparation, gates, memory, and readout of a trapped-ion quantum bit, Phys. Rev. Lett. **113**, 220501 (2014).

[28] R. Srinivas, S. C. Burd, H. M. Knaack, R. T. Sutherland, A. Kwiatkowski, S. Glancy, E. Knill, D. J. Wineland, D. Leibfried, A. C. Wilson, D. T. C. Allcock, and D. H. Slichter, High-fidelity laser-free universal control of trapped ion qubits, Nature **597**, 209 (2021).

[29] J. P. Gaebler, T. R. Tan, Y. Lin, Y. Wan, R. Bowler, A. C. Keith, S. Glancy, K. Coakley, E. Knill, D. Leibfried, and D. J. Wineland, High-fidelity universal gate set for ^{9}Be$^+$ ion qubits, Phys. Rev. Lett. **117**, 060505 (2016).

[30] C. R. Clark, H. N. Tinkey, B. C. Sawyer, A. M. Meier, K. A. Burkhardt, C. M. Seck, C. M. Shappert, N. D. Guise, C. E. Volin, S. D. Fallek, H. T. Hayden, W. G. Rellergert, and K. R. Brown, High-fidelity bell-state preparation with ^{40}Ca$^+$ optical qubits, Phys. Rev. Lett. **127**, 130505 (2021).

[31] B. B. Blinov, D. L. Moehring, L.-M. Duan, and C. Monroe, Observation of entanglement between a single trapped atom and a single photon, Nature **428**, 153 (2004).

[32] H.-X. Yang, J.-Y. Ma, Y.-K. Wu, Y. Wang, M.-M. Cao, W.-X. Guo, Y.-Y. Huang, L. Feng, Z.-C. Zhou, and L.-M. Duan, Realizing coherently convertible dual-type qubits with the same ion species, Nat. Phys. **18**, 1058 (2022).

[33] I. V. Inlek, C. Crocker, M. Lichtman, K. Sosnova, and C. Monroe, Multispecies trapped-ion node for quantum networking, Phys. Rev. Lett. **118**, 250502 (2017).

[34] V. Negnevitsky, M. Marinelli, K. K. Mehta, H.-Y. Lo, C. Flühmann, and J. P. Home, Repeated multi-qubit readout and feedback with a mixed-species trapped-ion register, Nature **563**, 527 (2018).

[35] D. M. Lucas, B. C. Keitch, J. P. Home, G. Imreh, M. J. McDonnell, D. N. Stacey, D. J. Szwer, and A. M. Steane, A long-lived memory qubit on a low-decoherence quantum bus (2007), arXiv:0710.4421.

[36] Sandia National Laboratories HOA2.

[37] See Supplemental Material.

[38] J. P. Home, M. J. McDonnell, D. J. Szwer, B. C. Keitch, D. M. Lucas, D. N. Stacey, and A. M. Steane, Memory coherence of a sympathetically cooled trapped-ion qubit, Phys. Rev. A **79**, 050305(R) (2009).

[39] C. J. Ballance, T. P. Harty, N. M. Linke, M. A. Sepiol, and D. M. Lucas, High-fidelity quantum logic gates using trapped-ion hyperfine qubits, Phys. Rev. Lett. **117**, 060504 (2016).

[40] M. A. Sepiol, A. C. Hughes, J. E. Tarlton, D. P. Nadlinger, T. G. Ballance, C. J. Ballance, T. P. Harty, A. M. Steane, J. F. Goodwin, and D. M. Lucas, Probing qubit memory errors at the part-per-million level, Phys. Rev. Lett. **123**, 110503 (2019).

[41] D. Kielpinski, B. E. King, C. J. Myatt, C. A. Sackett, Q. A. Turchette, W. M. Itano, C. Monroe, D. J. Wineland, and W. H. Zurek, Sympathetic cooling of trapped ions for quantum logic, Phys. Rev. A **61**, 032310 (2000).

[42] A. C. Hughes, V. M. Schäfer, K. Thirumalai, D. P. Nadlinger, S. R. Woodrow, D. M. Lucas, and C. J. Ballance, Benchmarking a high-fidelity mixed-species entangling gate, Phys. Rev. Lett. **125**, 080504 (2020).

[43] A. H. Myerson, D. J. Szwer, S. C. Webster, D. T. C. Allcock, M. J. Curtis, G. Imreh, J. A. Sherman, D. N. Stacey, A. M. Steane, and D. M. Lucas, High-fidelity readout of trapped-ion qubits, Phys. Rev. Lett. **100**, 200502 (2008).

[44] D. Main, *Magnetic Field Stabilisation in Ion Traps*, Master's thesis, University of Oxford (2020).

[45] C. D. Bruzewicz, R. McConnell, J. Stuart, J. M. Sage, and J. Chiaverini, Dual-species, multi-qubit logic primitives for Ca$^+$/Sr$^+$ trapped-ion crystals, npj Quantum Inf. **5**, 102 (2019).

[46] D. P. Nadlinger, P. Drmota, D. Main, B. C. Nichol, G. Araneda, R. Srinivas, L. J. Stephenson, C. J. Ballance, and D. M. Lucas, Micromotion minimisation by synchronous detection of parametrically excited motion (2021), arXiv:2107.00056.

[47] P.-J. Stas, Y. Q. Huan, B. Machielse, E. N. Knall, A. Suleymanzade, B. Pingault, M. Sutula, S. W. Ding, C. M. Knaut, D. R. Assumpcao, Y.-C. Wei, M. K. Bhaskar, R. Riedinger, D. D. Sukachev, H. Park, M. Lončar, D. S. Levonian, and M. D. Lukin, Robust multi-qubit quantum network node with integrated error detection (2022).

[48] J. Řeháček, Z. c. v. Hradil, E. Knill, and A. I. Lvovsky, Diluted maximum-likelihood algorithm for quantum tomography, Phys. Rev. A **75**, 042108 (2007).

[49] A. Anis and A. I. Lvovsky, Maximum-likelihood coherent-state quantum process tomography, New J. Phys. **14**, 105021 (2012).

[50] P. Badziag, M. Horodecki, P. Horodecki, and R. Horodecki, Local environment can enhance fidelity of quantum teleportation, Phys. Rev. A **62**, 012311 (2000).

[51] A. M. Souza, G. A. Álvarez, and D. Suter, Robust dynamical decoupling for quantum computing and quantum memory, Phys. Rev. Lett. **106**, 240501 (2011).

[52] C. Monroe, R. Raussendorf, A. Ruthven, K. R. Brown, P. Maunz, L.-M. Duan, and J. Kim, Large-scale modular quantum-computer architecture with atomic memory and photonic interconnects, Phys. Rev. A **89**, 022317 (2014).

[53] E. Megidish, A. Halevy, T. Shacham, T. Dvir, L. Dovrat, and H. S. Eisenberg, Entanglement swapping between photons that have never coexisted, Phys. Rev. Lett. **110**, 210403 (2013).

[54] C. H. Bennett, G. Brassard, S. Popescu, B. Schumacher, J. A. Smolin, and W. K. Wootters, Purification of noisy

entanglement and faithful teleportation via noisy channels, Phys. Rev. Lett. **76**, 722 (1996).

[55] C. Monroe and J. Kim, Scaling the ion trap quantum processor, Science **339**, 1164 (2013).

[56] R. Nigmatullin, C. J. Ballance, N. d. Beaudrap, and S. C. Benjamin, Minimally complex ion traps as modules for quantum communication and computing, New J. Phys. **18**, 103028 (2016).

[57] A. Broadbent, J. Fitzsimons, and E. Kashefi, Universal blind quantum computation, in *2009 50th Annual IEEE Symposium on Foundations of Computer Science* (2009) pp. 517–526.

[58] A. Stute, B. Casabone, B. Brandstätter, K. Friebe, T. E. Northup, and R. Blatt, Quantum-state transfer from an ion to a photon, Nat. Photon. **7**, 219 (2013).

[59] T. A. Wright, R. J. A. Francis-Jones, C. B. E. Gawith, J. N. Becker, P. M. Ledingham, P. G. R. Smith, J. Nunn, P. J. Mosley, B. Brecht, and I. A. Walmsley, Two-way photonic interface for linking the Sr$^+$ transition at 422 nm to the telecommunication C band, Phys. Rev. Applied **10**, 044012 (2018).

[60] V. Krutyanskiy, M. Meraner, J. Schupp, V. Krcmarsky, H. Hainzer, and B. P. Lanyon, Light-matter entanglement over 50 km of optical fibre, npj Quantum Inf. **5**, 72 (2019).

[61] J. Hannegan, J. D. Siverns, and Q. Quraishi, Entanglement between a trapped-ion qubit and a 780-nm photon via quantum frequency conversion, Phys. Rev. A **106**, 042441 (2022).

[62] S. Bourdeauducq *et al.*, m-labs/artiq: 6.0 (Version 6.0) (2021).